Hindawi
International Journal of Energy Research
Volume 2024, Article ID 8508691, 9 pages
https://doi.org/10.1155/2024/8508691

Research Article

Photonic Crystal-Integrated Semitransparent Solar Cell for Solar Greenhouse Application

Devina Thasia Wijaya, Yun Jae Eo, Young Rag Do, and Chan Woo Lee

Department of Chemistry, Kookmin University, Seoul 02707, Republic of Korea

Correspondence should be addressed to Young Rag Do; yrdo@kookmin.ac.kr and Chan Woo Lee; cwlee1@kookmin.ac.kr

Received 27 October 2023; Revised 20 February 2024; Accepted 15 April 2024; Published 30 April 2024

Academic Editor: Pawan Kumar Kulriya

Solar greenhouse technology emerges as a solution that intensifies crop yields and allows utilities to generate energy from photovoltaic cells. Here, we demonstrate a photonic crystal-integrated solar cell that selectively transmits photosynthetic light for plant cultivation and reflects the remaining light to the adjacent solar cells to generate electricity. The photonic crystal is fabricated using an e-beam evaporation method by nonperiodic stacking of TiO_2 and SiO_2 layers to transmit light at 400–500 nm (blue) and 600–700 nm (red) and reflect green (500–600 nm), ultraviolet, and infrared light. The photonic crystal-integrated solar cell is constructed with the vertically arranged copper indium gallium diselenide (CIGS) solar cell and the tilted photonic crystal with respect to the CIGS cell. By controlling the tilting angle of the photonic crystal film, it achieves the generated electric power of 40.2 W m^{-2} and the irradiance of 124.6 W m^{-2} for transmitted photosynthetic lights (400–500 and 600–700 nm). In contrast, a conventional horizontal CIGS cell shows a power generation of 55.6 W m^{-2} without any light transmission. This work provides a new optical strategy and design principle for the development of a wavelength-selective semitransparent solar cell.

1. Introduction

Controlled-environment agriculture, such as greenhouses and vertical farms, has been widely recognized as a primary solution for sustainable food production [1]. The crop yield can be maximized within the minimum space with efficient control of essential plant growing necessities, such as water, temperature, humidity, ventilation, light, and CO_2 [2, 3]. With the increasing number of industries implementing this idea, much greater energy is required to drive these microclimate controls. In addition, with the current high demand for land for renewable energy production, there is a high risk of food scarcity due to converting land usage from food farming to renewable energy farming [4–6]. Therefore, a more sustainable system is needed to ensure the food and energy demand.

One of the most recent technologies developed to satisfy these conditions is integrating photovoltaic technology with greenhouse operation [3, 7, 8] (i.e., solar greenhouse technology). With this technology, solar light is converted to electricity using a solar cell directly to drive the photosynthetic reaction in plants, outperforming traditional greenhouses in terms of carbon footprint [9]. The generated electricity can be used directly for greenhouse operations or exported to a power grid or battery when surplus energy is generated [10]. In this system, the primary role of the greenhouse cover/cladding materials is to direct the light into the internal environment of the greenhouse and toward the solar cells, in addition to protecting the interior from damaging UV light. For this purpose, many transparent solar cells for invisible energy harvesters can be adopted. For example, a lightweight and flexible Ga_2O_3/Cu_2O heterojunction can generate electric power with 1.66% power conversion efficiency (PCE) while delivering photovoltage of 900 mV with a power of 1.66 mW cm^{-2} [11]. This heterojunction allows for electric power generation while maintaining the UV and visible light-controlling properties of the material. In another work, a broadband energy harvester, integrated transparent photovoltaic-transparent heater (TPV-TH), simultaneously blocked ultraviolet (UV) rays and maintained 39% light

transmittance, while generating 6 mW onsite power which corresponds to 3% PCE under AM1.5G condition [12]. Interestingly, this concept of electricity generation from a transparent material can be further evolved by incorporating a color-tuning scheme. For example, color-tunable photovoltaic cells were reported to deliver onsite power for indoor applications [13]. The color can be tuned by controlling the thickness of the ZnO back reflector (BR) layer, thus performing a high efficiency of 3.8% under indoor light.

Accounting for the photosynthetically active radiation (PAR) mainly comprised of 400–500 (blue) and 600–700 nm (red) wavelengths [14], a successful greenhouse cover material should transmit light within this wavelength range [15–18]. While excessive direct solar radiation results in crop damage, limited radiation may inhibit plant growth. In addition, an appropriate cover design excludes undesirable light that are harmful to the plant, such as ultraviolet (UV), green, or near-infrared light, which can increase the temperature inside the greenhouse [14, 19]. Therefore, engineering the cover materials requires highly fine-tuned efforts that satisfy plant needs, which are unique for each plant [9, 19, 20].

Among many developed materials, photonic crystals, with their unique ability to manipulate the flow of light, present a revolutionary solution as greenhouse cover materials [21], particularly in optimizing plant growth through precise control of transmitted radiation. The tunability of photonic crystals allows for the selective transmission of crucial photosynthetically active radiation (PAR) while efficiently reflecting detrimental lights. Especially, significant advancements have been made in the field of multilayer photonic crystals employing nonabsorbing and nondispersive titanium dioxide (TiO_2) and silicon dioxide (SiO_2) which are widely used for visible range transmission [22]. The work by Kanehira et al. laid foundational insights into the fabrication and optical characteristics of TiO_2/SiO_2 multilayer structures [23]. Subsequent contributions delved into the optimization of layer thicknesses [22, 24], temperature evolution [25], and porosity [26] to achieve specific optical functionalities. This collective progress underscores the versatility and promise of the manipulable photonic response of TiO_2/SiO_2 multilayer photonic crystals and its adaptability as cover materials in a greenhouse.

In this work, we demonstrate a photonic crystal-integrated solar cell (PCISC) that selectively transmits photosynthetically efficient light for plant cultivation and reflects the remaining wavelengths to the integrated solar cells to produce electricity (Figure 1). To prepare the photonic crystal, we simulated a nonperiodic multilayer comprising TiO_2 and SiO_2 to transmit specific wavelengths (400–500 nm and 600–700 nm) [27]. Then, we fabricated it using electron beam evaporation on a glass substrate. The photonic crystal was installed with an inclined angle relative to a vertical solar cell to direct reflected light into the solar cell. The effects of a tilting angle on power generation and light transmission were studied. By applying the photonic crystal-integrated solar cell onto the virtual greenhouse roof, the photosynthetically active light can be illuminated with high irradiance while assuring a significant amount of power generation comparable to a conventional horizontal solar cell.

2. Materials and Methods

2.1. Photonic Crystal Simulation and Fabrication. The photonic crystals were designed and fabricated considering the wavelength range of light for plant photosynthesis as in previous publications [28, 29]. Briefly, the photonic crystals were designed to transmit the blue (450 nm) and red (660 nm) light while reflecting the green (550 nm) and infrared (>1000 nm) lights using the Essential Macleod simulation program (Thin Film Center, Inc., USA). In the simulation process, TiO_2 (with a high refractive index) and SiO_2 (with a low refractive index) were adopted as materials for the photonic crystal. All photonic crystal types were initially designed with the optical thickness of $(0.5SiO_2/TiO_2/0.5SiO_2)^n$, and refinement processes were performed to minimize the ripple at the baseline. Four types of photonic crystal were designed according to the transmission bands, (1) type 1 with transmission bands of 400–450 and 650–700 nm, (2) type 2 with transmission bands of 450–500 and 600–650 nm, (3) type 3 with transmission bands of 400–500 and 640–700 nm, and (4) type 4 with transmission bands of 400–500 and 600–700 nm, to obtain the photonic crystal that gives the highest transmission and reflection in the desired wavelength region. The SiO_2 and TiO_2 were then deposited accordingly, following the calculated nonperiodic sequence at a temperature of 250°C using an e-beam evaporator on a 10×10 cm glass substrate. The cross-section of the fabricated photonic crystals was confirmed using field-emission scanning electron microscopy (JSM-7610F, JEOL Ltd., Japan), and the transmittance was confirmed using UV-visible spectroscopy (LAMBDA 365, PerkinElmer, Inc., USA). The detailed simulated and fabricated layer thicknesses are shown in Table S1.

2.2. Photonic Crystal-Integrated Solar Cell Performance Measurement. Commercial CIGS thin-film solar cells (FLEX-03N, Miasolé Hi-Tech Corp., USA) with a cell efficiency of 17.0% in the dimensions of 2.5×15 cm were used to evaluate the performance of the solar cell with a photonic crystal. The light transmitted through the photonic crystal is used for photosynthesis in plants, and the light reflected through the photonic crystal is recycled in the CIGS solar cell. The photonic crystal was tilted with angle (θ) varying from 0 to 60°, as depicted in Figure 1. A custom-made holder held the photonic crystal-integrated solar cell on the top of a nickel tripod 11 cm in height (Figure S1). The solar illumination in this experiment was performed using a class A solar simulator with a power of a 150 W xenon lamp and illumination area of 10×10 cm (94022A, Newport Corporation, USA), and the light intensity was adjusted using a KG-5 filter-covered monosilicon detector calibrated by the National Renewable Energy Laboratory. The nominal lamp power was set to 144 W (0.85 SUN) to match the upper limit of light irradiance detection using the spectrophotometer (CL-500A, Konica Minolta, Japan). The spectrophotometer was placed under the nickel tripod with the primary light sensor directly illuminated by the light from the solar simulator. The distance between the solar simulator light source to the spectrophotometer and photonic crystal was fixed at 23 and

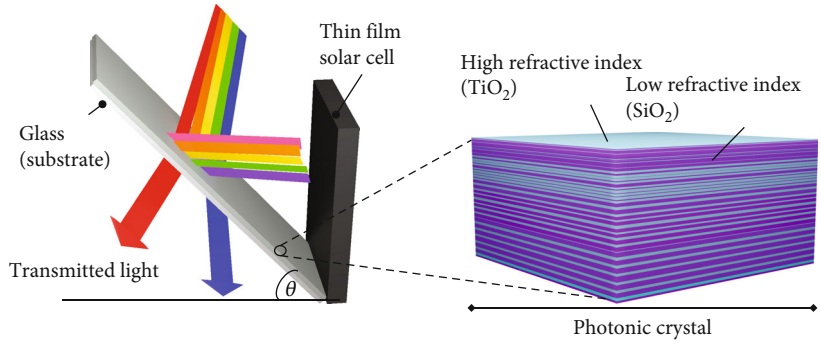

FIGURE 1: Schematic of the photonic crystal-integrated solar cell for solar greenhouse technology. The photonic crystal selectively transmits red and blue lights for crop photosynthesis, while ultraviolet (UV), green, yellow, and infrared (IR) lights are reflected using the optical photonic crystal and supplied to thin-film solar cells. The photonic crystal was set at various tilting angles (θ) to direct reflected light into the solar cell for electricity generation.

12 cm, respectively. From this experiment, the generated power was calculated from the measured short circuit current (I_{SC}) and open circuit potential (V_{OC}), which were then normalized by the illumination area of the solar cell, which is 5×10 cm, multiplied by the fill factor ($FF_{\text{solar cell}}$) obtained from the product specification on Table S2.

$$\text{Generated power}\left(\text{Wm}^{-2}{}_{\text{solar cell}}\right) = \text{FF}_{\text{solar cell}} \times \frac{I_{SC} \times V_{OC}}{0.005}. \quad (1)$$

On the other hand, irradiance value was obtained by integrating the spectral irradiance within the regions 400 to 500 and 600 to 700 nm to represent the PAR light.

$$\text{Irradiance}\left(\text{Wm}^{-2}\right) = \int_{400}^{500} E_{e,\lambda} d\lambda + \int_{600}^{700} E_{e,\lambda} d\lambda. \quad (2)$$

In addition, since we cannot fully measure the irradiance of the simulated solar power, the power conversion efficiency (PCE) value obtained from our experiment was calculated by the following equation:

$$\text{PCE}(\%) = \frac{\text{generated power}}{\text{solar irradiance}}, \quad (3)$$

where generated power is calculated by equation (1) and solar irradiance equals 0.85 SUN (0.85 fraction of AM1.5G full spectrum power of 1000 W m^{-2}, which was an assumption based on the integrated transmittance spectra measured from 144 W of lamp power). For the PCISC configuration, the solar irradiance was obtained by subtracting the measured total irradiance of the transmitted light (under 380 to 780 nm region) from the solar irradiance of 0.85 SUN.

3. Results and Discussion

Figure 1 demonstrates a schematic of the photonic crystal-integrated solar cell for solar greenhouse application. The optical properties of the one-dimensional photonic crystals (1DPC) can be tuned by designing its stacking components to only reflect a specific wavelength range [27–32]. The lights reflected by the photonic crystal are absorbed by the thin-film solar cells to generate electrical power, which can be employed for greenhouse operation. The CIGS solar cell was used as the model solar cell because it allows for light absorption with a high-power conversion efficiency in a broader wavelength range [33].

It is known that blue (400–500 nm) and red (600–700 nm) lights of the PAR constitute the light absorbed by plants to carry out photosynthetic reactions (Figure 2(a)) [14]. Photosynthetic reactions efficiently occur when important photosynthesis pigments such as chlorophyll a, chlorophyll b, and carotenoids absorb light under these blue and red regions [34, 35]. Additionally, in some cases, the illumination of green light (500-600 nm) hinders the growth of plants and lowers the photosynthates such as protein and starches [36]. Therefore, the structural design of photonic crystal thin films was simulated to selectively transmit the red and blue lights. Four types of photonic crystal were designed in this study: types 1, 2, 3, and 4. Each type was designed to transmit light with different center wavelengths and bandwidths at the wavelength regions of 400-500 nm (blue) and 600-700 nm (red) (Figure 2(b)). The simulation is based on the constructive and destructive optical interferences produced within a multilayer thin film comprising high and low refractive index materials [28, 29, 37, 38].

The photonic crystals were fabricated using an e-beam evaporator to deposit SiO_2 (theoretical refractive index = 1.46) and TiO_2 (theoretical refractive index = 2.31) layers nonperiodically on a 10×10 cm transparent glass substrate to maximize the light-transmitting property of the photonic crystal. The e-beam evaporator method is used because of its capability to create high resolution structures with intricate and precise features with direct writing and rapid prototyping capability [39]. For type 1 1DPC, a total of 52 layers consisting of TiO_2 and SiO_2 were deposited according to the simulated thickness (Figure 2(c)). Meanwhile, 62 layers for type 2 (Figure 2(d)) and 60 layers for type 3 and 4 1DPC (Figures 2(e) and 2(f), respectively) were deposited; the thicknesses of each layer is provided in Table S1, where layer #1 corresponds to the starting layer. The detailed analysis results of material characterization on the photonic crystal thin films can be found in Figure S2

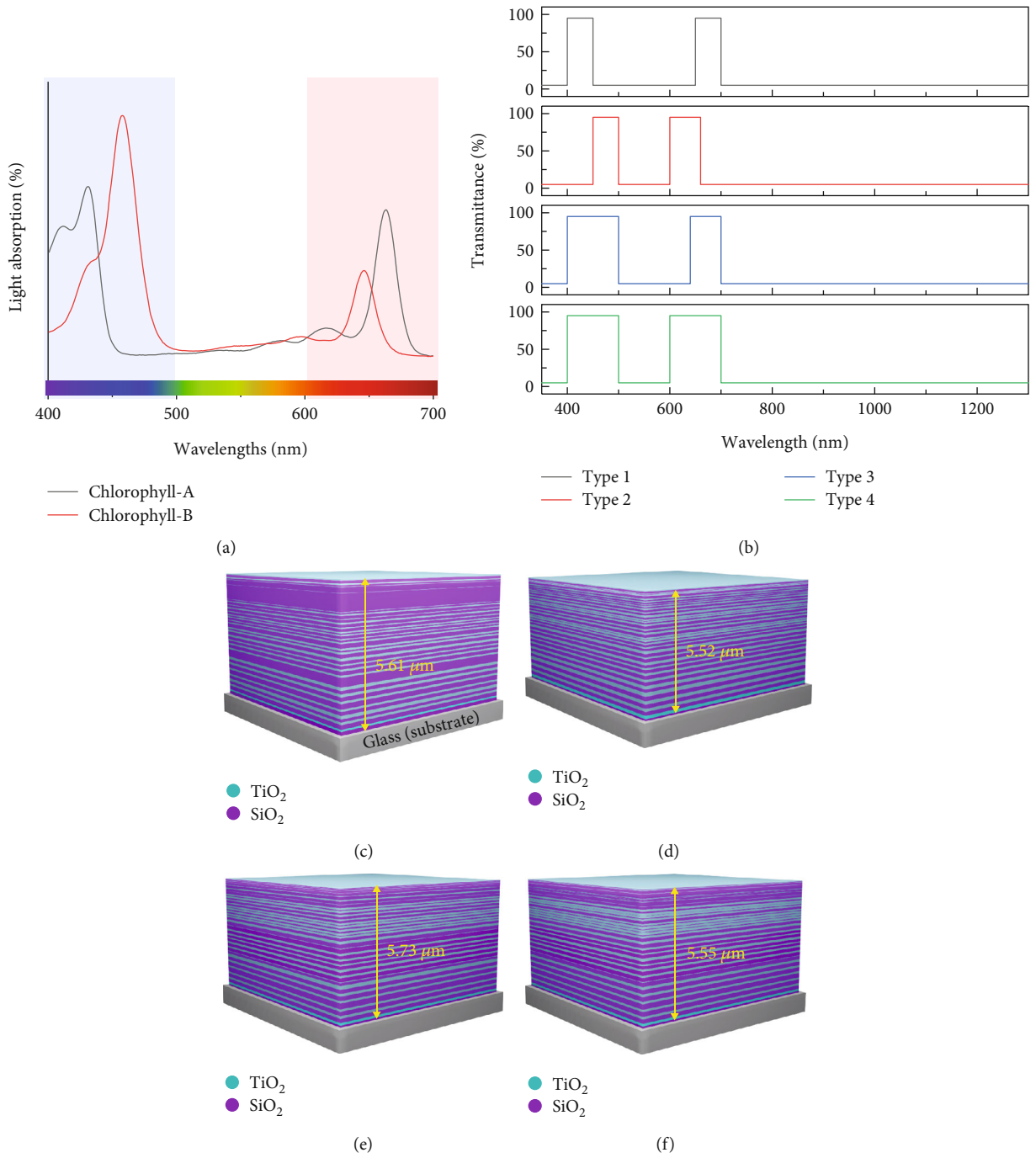

Figure 2: (a) Light absorption spectrum of photosynthesis pigments, such as chlorophyll a and chlorophyll b, as a function of wavelength, redrawn from Ref. [40, 41]. (b) Transmittance spectra of various photonic crystals (types 1, 2, 3, and 4) designed for the selective transmission of red and blue lights for photosynthetic reactions. Schematic models of the designed nonperiodic stacking layer of (c) type 1, (d) type 2, (e) type 3, and (f) type 4 photonic crystals. Blue color represents high refractive index TiO_2, and purple represents low refractive index SiO_2.

(reproduced with permission from Ref. [32]). These deposited layers yield total thicknesses of 5.61, 5.62, 5.73, and 5.55 μm with an average per layer thickness error of 8.18, 10.72, 7.83, and 7.99 nm for type 1, 2, 3, and 4 1DPC, respectively (Figure S3). The significant contrast of refractive indices between SiO_2 and TiO_2 enables the production of narrowband and pure colors by combinatorically optimizing the layer structural parameters, such as the thickness, stacking order, number of stacking pairs, and periodicity of the high- and low-index layers [27]. The nonperiodic stacking layer photonic crystal yields enhanced color purity with the minimum baseline of ripple-shape patterns [27, 32], which is crucial for selectively transmitting photosynthetic active light.

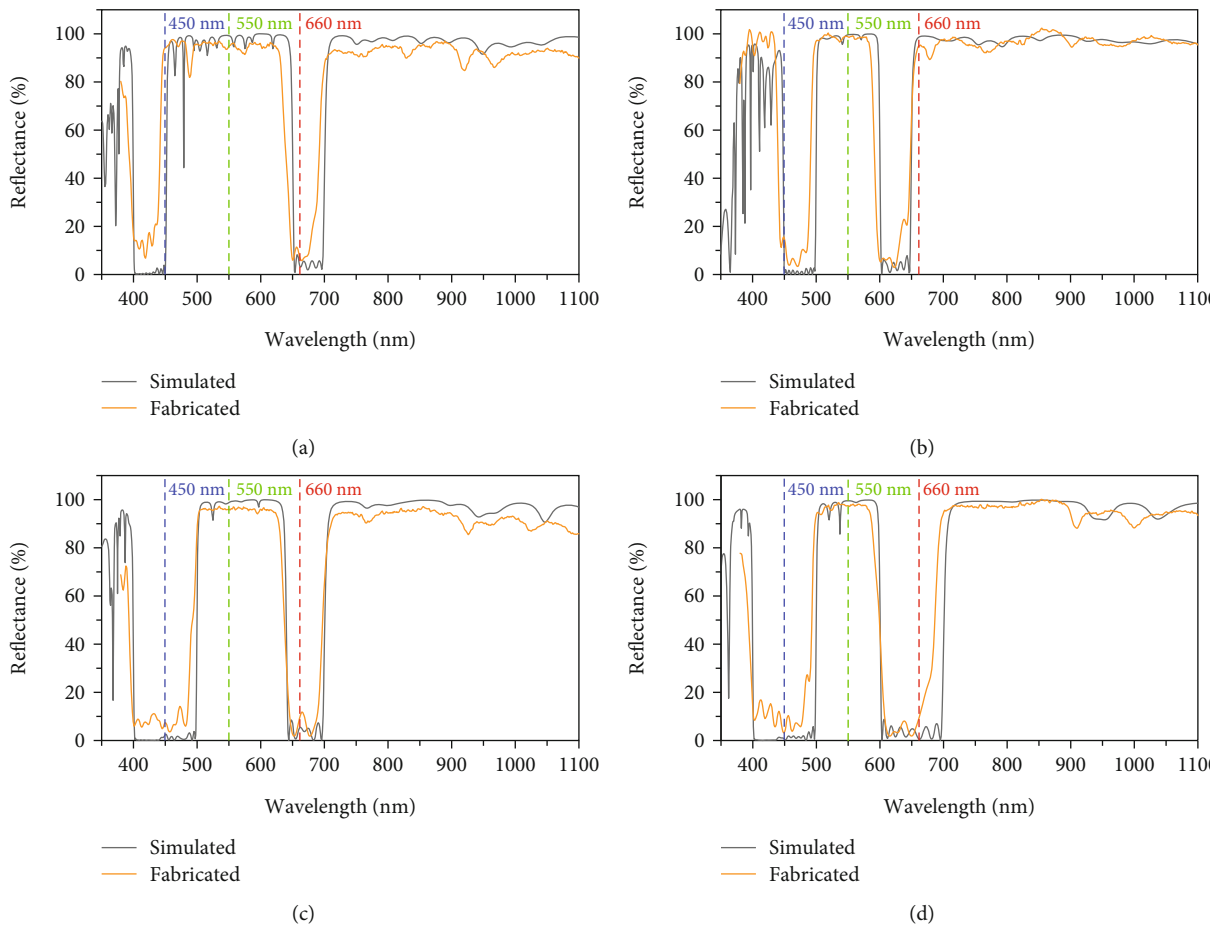

Figure 3: Reflectance spectra of (a) type 1, (b) type 2, (c) type 3, and (d) type 4 photonic crystals. Dashed blue, green, and red lines represent wavelengths of 450, 550, and 660 nm, respectively. The low reflectance values at the wavelength regions of red and blue lights represent selective transmission of photosynthetically active radiation.

In Figure 3 and Figure S4, reflectance and transmittance spectra are presented for both simulated and fabricated photonic crystals. For type 1 1DPC, only 14.4% and 7.9% reflectances were measured under 400-450 nm and 650-700 nm spectral region, while the simulated reflectance values were 1.0% and 4.3%, respectively. Conversely, within the wavelength range of 450-650 nm, the 1DPC exhibited a reflectance of 94.8%, slightly below the simulated value of 97.3%. In type 2 1DPC, a comparatively lower reflectance value of 9.4% and 10.5% was obtained under 450-500 nm and 600-650 nm regions, which also substantially deviated from the simulated values of 1.3% and 3.8%. However, a notably high reflectance of 98.2% was achieved under 500-600 nm region, closely approaching the target reflectance of 98.8% in the same wavelength region. Meanwhile, under 400-500 nm region, type 3 and 4 1DPC reflect only 8 to 9% of light, while maintaining low reflectance of approximately 5.9% at 650-700 nm (type 3) and 600-700 nm (type 4). Furthermore, these filters demonstrated a high reflectance up to 97% under 500-600 nm region.

The reflectance spectra suggest that the fabricated photonic crystals successfully reflect the targeted wavelengths as simulated in all spectra, with only <4% shift from the target wavelength. Among all fabricated photonic crystals, the type 4 photonic crystal exhibited the appropriate bandwidths around the wavelengths of blue (450 nm) and red (660 nm) lights (Figure 3(d)), which are the primary target wavelengths for greenhouse operations. It can be identified that the band center is positioned at 450 and 650 nm with a bandwidth of approximately 100 nm for the transmission of blue and red light. Moreover, the band center for the reflection of green light is placed at 550 nm with a bandwidth of 100 nm. Furthermore, the high reflectance at wavelengths higher than 780 nm indicates that these photonic crystals successfully reflect near-infrared light, which can be used for CIGS solar cells with a narrow bandgap. The reflection of near-infrared light can also help to increase energy efficiency in greenhouse operation because infrared light could require excessive cooling [7, 42, 43].

The photonic crystal-integrated solar cell was constructed with a vertical solar cell and a tilted photonic crystal (type 4) as illustrated in Figure S1. Spectral irradiance of transmitted solar light, following its passage through the tilted photonic crystal, was measured using a spectrophotometer positioned beneath the crystal. Concurrently, the solar cells were linked to a portable multimeter to quantify generated power. The

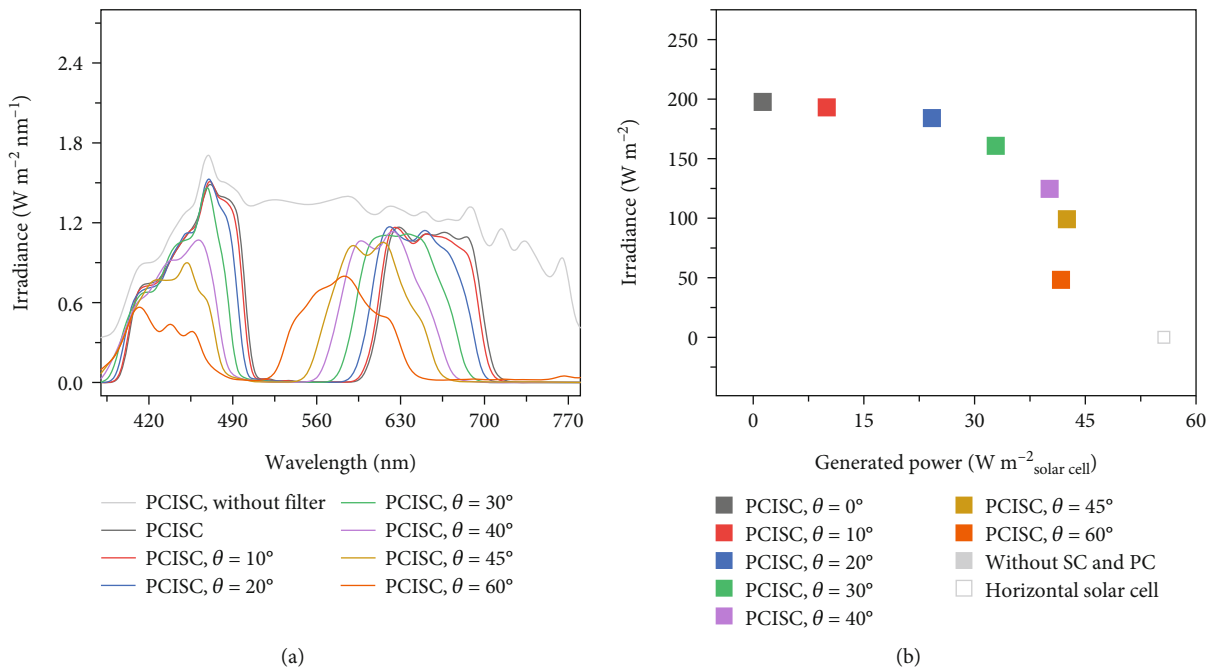

FIGURE 4: (a) Spectral irradiance of transmitted solar light, following its passage through the photonic crystal-integrated solar cell (PCISC). (b) The plot of irradiance and generated power measured with different tilting angles (θ) of the photonic crystal. The irradiance value is obtained with the integration of spectral irradiance with respect to the wavelength range of red and blue lights (400-500 and 600-700 nm). The generated power is obtained by multiplying the voltage and current measured from the solar cell. The photonic crystal-integrated solar cell shows superior performances in terms of power generation and PAR illumination, compared to the conventional horizontal solar cell.

irradiation of the solar spectrum was performed using a solar simulator. The selection of a commercial CIGS solar cell was based on its capacity for light absorption across a wide wavelength range of 400 to 1100 nm [44, 45]. A summary of the reported cell efficiency and performance is provided in Table S2.

As presented in Figure 4(a), tilting the photonic crystal resulted in the wavelength shift and the intensity decrease of transmitted light. This phenomenon arises from variations in the incident light angle, causing different light reflection and refraction interference between the multilayer interfaces or Bragg stack within the photonic crystal coating [29, 37, 46]. Nevertheless, it is intriguing to note that the tilting of the photonic crystal facilitates the generation of electricity by the solar cell (Figure 4(b)). Systematic variation of the tilt angle from 0 to 45° resulted in an increase of the generated power from 1.46 to 44.35 W m^{-2}. This improvement results from the capability of the inclined photonic crystal to redirect reflected solar irradiation toward the solar cell. Consequently, a greater proportion of residual light penetrates the light absorption region of the solar cell, thereby resulting in an elevation of the generated electricity [47, 48]. In summation, the photonic crystal-integrated solar cell generates electricity in the cost of transmittance.

By setting the tilting angle at 40°, PCISC achieves a generated electric power of 40.2 W m^{-2} and the irradiance of 124.6 W m^{-2} for transmitted photosynthetic lights (400–500 and 600–700 nm). In contrast, a conventional horizontal CIGS cell shows the power generation of 55.6 W m^{-2} without any light transmission. This power generation is equivalent to 6.55% power conversion efficiency (PCE) considering the lower nominal lamp power used which is 144 W. Without photonic crystals and solar cells (denoted as without SC and PC in Figure 4(b)), the irradiance for transmitted photosynthetic lights was measured to be 239.3 W m^{-2}. Therefore, the photonic crystal-integrated solar cell enables about 72.3% of its maximum capability for electricity generation, which corresponds to 5.75% PCE, while still allowing the irradiation of blue and red lights. These results show that the light-guiding technology that utilizes photonic crystal is useful for solar greenhouse applications, as it exceeds the PCE records from present works about transparent photovoltaic (TPV) applications for self-sustain building [11–13]. However, for the harsh environment in the greenhouse applications, it is necessary to ensure the stability of the metal oxide layers composing the photonic crystal stability. Therefore, further study about the encapsulation process to ensure high permeability and chemical stability will be conducted in the future.

4. Conclusions

In summary, we simulated 1-D photonic crystals composed of a nonperiodic multilayer of SiO_2 and TiO_2 to design a photonic crystal that not only selectively transmits red and blue lights for photosynthesis and but also reflects UV, green, yellow, and infrared lights for electricity

generation by CIGS solar cells. The photonic crystal was prepared with an e-beam evaporation method on a glass substrate. The developed photonic crystal can deliver high transmittance for solar light in the PAR (400–500 and 600–700 nm) into the greenhouse interior while reflecting the remaining wavelengths. When the tilted photonic crystal was integrated with vertically arranged CIGS solar cells under simulated solar light, it made up 72.3% of the electricity power generated from horizontally placed solar cells. It allowed the transmission of PAR light at moderate levels of 52.1% to promote crop cultivation. Especially, when tilting the type 4 filter at 40°, 40.2 W m^{-2} electric power can be generated while maintaining 124.6 W m^{-2} irradiance of PAR light, which corresponds to 5.75% PCE. This proof of concept proposes an alternative cover material for solar greenhouse to realize new possibilities to elevate crop yields with net-zero emissions in the agricultural field.

Data Availability

The data used to support the findings of this study are included within the article.

Conflicts of Interest

The authors declare that there is no conflict of interest regarding the publication of this paper.

Acknowledgments

This work was supported by the Korea Institute of Planning and Evaluation for Technology in Food, Agriculture and Forestry (IPET) and Korea Smart Farm R&D Foundation (KosFarm) through Smart Farm Innovation Technology Development Program, funded by the Ministry of Agriculture, Food and Rural Affairs (MAFRA) and Ministry of Science and ICT (MSIT), Rural Development Administration (RDA) (No. RS-2024-00402759). This work was supported by the National Research Foundation of Korea (NRF) grant funded by the Korean Government (MSIT) (RS-2023-00210114 and NRF-2022R1A4A1019296).

Supplementary Materials

Table S1: thickness profile of layers in photonic crystal types 1, 2, 3, and 4. Table S2: efficiency table of CIGS solar cells. Figure S1: (a) scheme and (b) picture of experimental setup for semi-transparent solar cells measurement. Figure S2: SEM characterization of the fabricated (a) type 1, (b) type 2, (c) type 3, and (d) type 4 photonic crystals. Figure S3: the difference of the simulated and fabricated thicknesses of each layer for (a) type 1, (b) type 2, (c) type 3, and (d) type 4 photonic crystals. Figure S4: transmittance spectra of the simulated (black line) and fabricated (red line) (a) type 1, (b) type 2, (c) type 3, and (d) type 4 photonic crystals. *(Supplementary Materials)*

References

[1] C. Vatistas, D. D. Avgoustaki, and T. Bartzanas, "A systematic literature review on controlled-environment agriculture: how vertical farms and greenhouses can influence the sustainability and footprint of urban microclimate with local food production," *Atmosphere*, vol. 13, no. 8, p. 1258, 2022.

[2] C. Zisis, E. M. Pechlivani, S. Tsimikli, E. Mekeridis, A. Laskarakis, and S. Logothetidis, "Organic photovoltaics on greenhouse rooftops: effects on plant growth," *Materials Today: Proceedings*, vol. 21, pp. 65–72, 2019.

[3] F. Maureira, K. Rajagopalan, and C. O. Stöckle, "Evaluating tomato production in open-field and high-tech greenhouse systems," *Journal of Cleaner Production*, vol. 337, article 130459, 2022.

[4] T. Sekiyama and A. Nagashima, "Solar sharing for both food and clean energy production: performance of agrivoltaic systems for corn, a typical shade-intolerant crop," *Environments*, vol. 6, no. 6, p. 65, 2019.

[5] S. Bouckaert, A. F. Pales, C. McGlade et al., "Net zero by 2050: A roadmap for the global energy sector," 2021, https://www.iea.org/events/net-zero-by-2050-a-roadmap-for-the-global-energy-system.

[6] S. Edouard, D. Combes, M. Van Iseghem, M. N. W. Tin, and A. J. Escobar-Gutiérrez, "Increasing land productivity with agriphotovoltaics: application to an alfalfa field," *Applied Energy*, vol. 329, article 120207, 2023.

[7] O. Abedrabboh, M. Koç, and Y. Biçer, "Modelling and analysis of a renewable energy-driven climate-controlled sustainable greenhouse for hot and arid climates," *Energy Conversion and Management*, vol. 273, article 116412, 2022.

[8] R. A. Gonocruz, S. Uchiyama, and Y. Yoshida, "Modeling of large-scale integration of agrivoltaic systems: impact on the Japanese power grid," *Journal of Cleaner Production*, vol. 363, article 132545, 2022.

[9] S. Moretti and A. Marucci, "A photovoltaic greenhouse with variable shading for the optimization of agricultural and energy production," *Energies*, vol. 12, no. 13, p. 2589, 2019.

[10] H. Dinesh and J. M. Pearce, "The potential of agrivoltaic systems," *Renewable and Sustainable Energy Reviews*, vol. 54, pp. 299–308, 2016.

[11] N. Kumar, M. Patel, J. Kim, C. Jeong, and C. Wong, "Flexible transparent photovoltaics for ultra-UV photodetection and functional UV-shielding based on Ga_2O_3/Cu_2O heterojunction," *Applied Materials Today*, vol. 29, article 101620, 2022.

[12] M. Patel, S. Kim, and J. Kim, "Field-induced transparent electrode-integrated transparent solar cells and heater for active energy windows: broadband energy harvester," *Advanced Science*, vol. 10, no. 26, article e2303895, 2023.

[13] S. Kim, M. Patel, S. Youn, Y. Kim, K. Lee, and J. Kim, "Color-tunable transparent photovoltaics for onsite power production under sunlight and indoor light," *Materials Today Energy*, vol. 31, article 101203, 2023.

[14] C. Lamnatou and D. Chemisana, "Solar radiation manipulations and their role in greenhouse claddings: fluorescent solar concentrators, photoselective and other materials," *Renewable and Sustainable Energy Reviews*, vol. 27, pp. 175–190, 2013.

[15] Y. Zhai, Y. Ma, S. N. David et al., "Scalable-manufactured randomized glass-polymer hybrid metamaterial for daytime radiative cooling," *Science*, vol. 355, no. 6329, pp. 1062–1066, 2017.

[16] E. J. Baeza, A. J. B. van Breugel, S. Hemming, and C. Stanghellini, "Smart greenhouse covers: a look into the future," *Acta Horticulturae*, vol. 1268, pp. 213–224, 2020.

[17] J. Zorz, W. D. L. Richardson, A. Laventure et al., "Light manipulation using organic semiconducting materials for enhanced photosynthesis," *Cell Reports Physical Science*, vol. 2, no. 4, article 100390, 2021.

[18] Q. Ma, Y. Zhang, G. Wu et al., "Photovoltaic/spectrum performance analysis of a multifunctional solid spectral splitting covering for passive solar greenhouse roof," *Energy Conversion and Management*, vol. 251, article 114955, 2022.

[19] S. Hemming, "Use of natural and artificial light in horticulture-interaction of plant and technology," *Acta Horticulturae*, vol. 907, no. 907, pp. 25–35, 2011.

[20] D. Mazzeo, C. Baglivo, S. Panico, and P. M. Congedo, "Solar greenhouses: climates, glass selection, and plant well-being," *Solar Energy*, vol. 230, pp. 222–241, 2021.

[21] S. Y. Jeong, C. Y. Tso, J. Ha et al., "Field investigation of a photonic multi-layered TiO_2 passive radiative cooler in sub-tropical climate," *Renewable Energy*, vol. 146, pp. 44–55, 2020.

[22] S. Jena, R. B. Tokas, P. Sarkar et al., "Omnidirectional photonic band gap in magnetron sputtered TiO_2/SiO_2 one dimensional photonic crystal," *Thin Solid Films*, vol. 599, pp. 138–144, 2016.

[23] S. Kanehira, S. Kirihara, and Y. Miyamoto, "Fabrication of TiO_2–SiO_2 photonic crystals with diamond structure," *Journal of the American Ceramic Society*, vol. 88, no. 6, pp. 1461–1464, 2005.

[24] R. S. Dubey and V. Ganesan, "Reflectance modulation using SiO_2/TiO_2 multilayer structures prepared by sol-gel spin coating process for optical applications," *Superlattices and Microstructures*, vol. 111, pp. 1099–1103, 2017.

[25] G. Christidis, O. B. Fabrichnaya, S. M. Koepfli et al., "Photonic response and temperature evolution of SiO_2/TiO_2 multilayers," *Journal of Materials Science*, vol. 56, no. 33, pp. 18440–18452, 2021.

[26] A. García-Valenzuela, C. López-Santos, V. Rico, R. Alvarez, A. Palmero, and A. R. González-Elipe, "Environmentally tight TiO2–SiO2Porous 1D-photonic structures," *Advanced Materials Interfaces*, vol. 6, no. 4, article 1801212, 2019.

[27] G. Y. Yoo, R. Azmi, C. Kim et al., "Stable and colorful perovskite solar cells using a nonperiodic SiO_2/TiO_2 multinanolayer filter," *ACS Nano*, vol. 13, no. 9, pp. 10129–10139, 2019.

[28] Y. J. Eo, S. Kim, K. N. Lee et al., "Fabrication of circadian light meter with non-periodic optical filters to evaluate the non-visual effects of light on humans," *Applied Sciences*, vol. 11, no. 18, p. 8283, 2021.

[29] A. Haryanto, Y. J. Eo, Y. R. Do, and C. W. Lee, "Layer-by-layer assembly of 1-D photonic crystal for wavelength-selective optical filter," *Applied Surface Science*, vol. 611, article 155762, 2023.

[30] H. Shen, Z. Wang, Y. Wu, and B. Yang, "One-dimensional photonic crystals: fabrication, responsiveness and emerging applications in 3D construction," *RSC Advances*, vol. 6, no. 6, pp. 4505–4520, 2016.

[31] P. Lova, G. Manfredi, D. Comoretto, P. Lova, D. Comoretto, and G. Manfredi, "Advances in functional solution processed planar 1D photonic crystals," *Advanced Optical Materials*, vol. 6, no. 24, article 1800730, 2018.

[32] Y. J. Eo, S. Kim, J. H. Oh et al., "Development of PAR sensor applicable to greenhouses and smart farms using a ripple-free red/blue TiO_2/SiO_2dual-band bandpass filter," *ACS Applied Electronic Materials*, vol. 4, no. 12, pp. 6125–6132, 2022.

[33] W. Liu, H. Li, B. Qiao, S. Zhao, Z. Xu, and D. Song, "Highly efficient CIGS solar cells based on a new CIGS bandgap gradient design characterized by numerical simulation," *Solar Energy*, vol. 233, pp. 337–344, 2022.

[34] L. Guidi, M. Tattini, and M. Landi, "How does chloroplast protect chlorophyll against excessive light?," *Chlorophyll*, vol. 21, pp. 21–36, 2017.

[35] W. Shang, Y. Song, C. Zhang et al., "Effects of light quality on growth, photosynthetic characteristics, and endogenous hormones in in vitro-cultured Lilium plantlets," *Horticulture, Environment, and Biotechnology*, vol. 64, no. 1, pp. 65–81, 2023.

[36] N. Yavari, R. Tripathi, B. Wu, S. MacPherson, J. Singh, and M. Lefsrud, "The effect of light quality on plant physiology, photosynthetic, and stress response in *Arabidopsis thaliana* leaves," *PloS One*, vol. 16, no. 3, article e0247380, 2021.

[37] J. Shao, G. Liu, and L. Zhou, "Biomimetic nanocoatings for structural coloration of textiles," *Active Coatings for Smart Textiles*, pp. 269–299, 2016, https://www.sciencedirect.com/science/article/abs/pii/B9780081002636000125.

[38] J. Wu, J. Tu, K. Hu et al., "Sol–gel-derived bayberry-like SiO_2@TiO_2 multifunctional antireflective coatings for enhancing photovoltaic power generation," *Colloids and Surfaces A: Physicochemical and Engineering Aspects*, vol. 654, article 130173, 2022.

[39] Z. Wang and Z. Zhang, "Electron beam evaporation deposition," *Advanced Nano Deposition Methods*, pp. 33–58, 2016, https://onlinelibrary.wiley.com/doi/abs/10.1002/9783527696406.ch2.

[40] L. A. Clementson and B. Wojtasiewicz, "Dataset on the absorption characteristics of extracted phytoplankton pigments," *Data in Brief*, vol. 24, article 103875, 2019.

[41] E. Janeeshma, R. Johnson, M. S. Amritha et al., "Modulations in chlorophyll a fluorescence based on intensity and spectral variations of light," *International Journal of Molecular Sciences*, vol. 23, no. 10, p. 5599, 2022.

[42] K. S. Kumar, K. N. Tiwari, and M. K. Jha, "Design and technology for greenhouse cooling in tropical and subtropical regions: a review," *Energy and Buildings*, vol. 41, no. 12, pp. 1269–1275, 2009.

[43] D. Schwarz, A. J. Thompson, and H. P. Kläring, "Guidelines to use tomato in experiments with a controlled environment," *Frontiers in Plant Science*, vol. 5, article 81576, 2014.

[44] G. M. Wilson, M. Al-Jassim, W. K. Metzger, and D. Dimova-Malinovska, "The state-of-the-art and future development of the photovoltaic technologies – the route from crystalline to nanostructured and new emerging materials," *Journal of Physics: Conference Series*, vol. 253, no. 1, article 012007, 2010.

[45] S. H. Moon, S. J. Park, S. H. Kim et al., "Monolithic DSSC/CIGS tandem solar cell fabricated by a solution process," *Scientific Reports*, vol. 5, no. 1, pp. 1–6, 2015.

[46] K. C. Krogman, R. E. Cohen, P. T. Hammond, M. F. Rubner, and B. N. Wang, "Industrial-scale spray layer-by-layer assembly for production of biomimetic photonic systems," *Bioinspiration and Biomimetics*, vol. 8, no. 4, article 045005, 2013.

[47] M. Bilal, M. N. Arbab, M. Z. Afridi, and A. Khattak, "Increasing the output power and efficiency of solar panel by using

concentrator photovoltaics (CPV)," *International Journal of Engineering Works*, vol. 3, no. 12, pp. 98–102, 2016.

[48] D. Rana, G. Kumar, and A. R. Gupta, "Increasing the Output Power and Efficiency of Solar Panel by Using Concentrator Photovoltaic (CPV) and Low Cost Solar Tracker," in *2018 4th International Conference on Computational Intelligence & Communication Technology (CICT)*, pp. 1–5, Ghaziabad, India, 2018.